International Journal of Advances in Engineering and Management (IJAEM)
Volume 4, Issue 2 Feb 2022, pp: 1279-1286 www.ijaem.net ISSN: 2395-5252

On-line Evaluation of the Operating Mechanism of Circuit Breaker Opening and Closing Coils Based on Multi-physics System

Jiaxin Yuan[1], Chunhang Zou[1], Xinyi Yang[1], Jun Zhan[2]
[1]*School of Electrical Engineering and Automation, Wuhan University, Wuhan, Hubei, China*
[1]*School of Electrical Engineering and Automation, Wuhan University, Wuhan, Hubei, China*
[1]*School of Electrical Engineering and Automation, Wuhan University, Wuhan, Hubei, China*
2 China Southern Power Grid Shenzhen Power Supply Bureau Co. Ltd, Shenzhen, Guangdong, China

Submitted: 10-02-2022 Revised: 22-02-2022 Accepted: 25-02-2022

ABSTRACT
Traditional online evaluation methods for the state of the opening and closing coil operating mechanism of the circuit breaker can only analyse the opening and closing time, but lack the analysis of stroke force. In this paper, a three-dimensional finite element simulation model is established of the circuit breaker opening and closing coil of a certain type, and the coil current in the working process after the coil is energized is simulated and calculated, and the opening and closing time and stroke force are obtained. The simulation results are compared with the experimental results to verify the effectiveness of the finite element simulation modelling method presented in this paper. On the basis of simulation, some optimization suggestions are put forward to improve the performance of the opening and closing coil.

Keywords: opening and closing coil; opening and closing time; stroke-force; three-dimensional finite element simulation.

I. INTRODUCTION

Circuit breakers are the core equipment for power grid protection and control, and timely detection of their mechanical failures is the basis for ensuring the safe and stable operation of the power grid[1-2]. The opening and closing coil is a core component of the circuit breaker. Once the opening and closing coil fails, the operating mechanism of the circuit breaker will not operate properly, which will further widen the power outage accident. In the process of the opening and closing coil operation, the opening and closing time and stroke-force can best reflect its operating transient characteristics[3], but the research on stroke-force is not sufficient currently.

The detection methods for opening and closing time and stroke-force of opening and closing coils at home and abroad are mainly divided into two categories: direct detection and indirect detection. The direct detection method is generally suitable for the maintenance and quality inspection of the factory product[4-6]. This method requires the equipment to be disassembled for experiments after the power is off, which is not conducive to maintaining the reliability of the power supply. In addition, the internal space of the opening and closing coil is small, so it is not suitable to install a sensor device inside for direct detection.

Indirect detection is mainly divided into two categories: mechanical signal based or electrical signal based[7-9]. Vibration signal is easily affected by the structure of the circuit breaker, various environmental noises and other factors. The most widely used detection method is the indirect measurement method based on the coil current signal. The current signal includes not only the opening and closing time, but also the status information of multiple mechanisms such as coil, electromagnet, and mechanical transmission[10]. This paper proposes a three-dimensional finite element simulation modelling method, which can quantitatively calculate the stroke-force and opening and closing time.

International Journal of Advances in Engineering and Management (IJAEM)
Volume 4, Issue 2 Feb 2022, pp: 1279-1286 www.ijaem.net ISSN: 2395-5252

II. OPERATING PROCESS OF OPENING AND CLOSING COIL

Fig. 1 shows the circuit breaker operation principle, in which 1 is the closing coil and 7 is the opening coil. After the coil is energized, the iron core of the closing coil or opening coil action hits the blurt device, making the operating mechanism of the circuit breaker move to complete closing and opening. The opening coil and closing coil work in the same mechanism, which are similar in structure and power source. In the subsequent analysis of this article, we collectively refer to them as the opening and closing coil. The structure of a typical opening and closing coil is shown in Fig. 2, and the equivalent circuit is shown in Fig. 3.

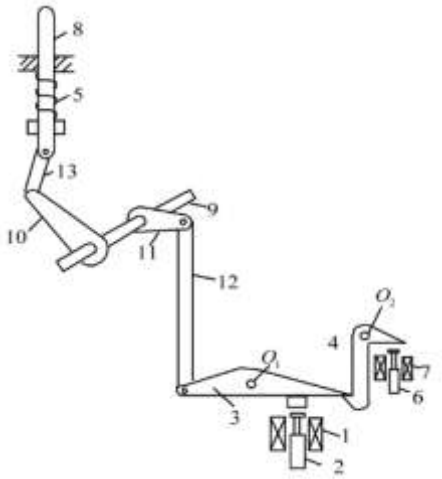

Fig. 1 Circuit breaker working diagram

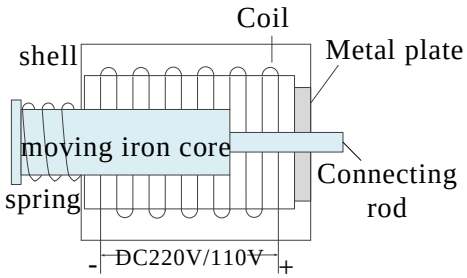

Fig. 2 Internal structure of the opening and closing coil

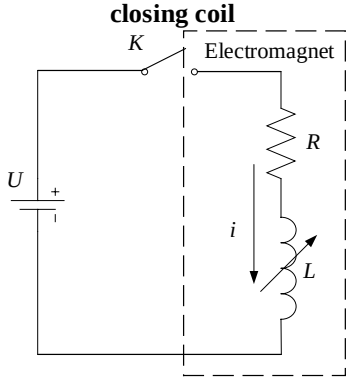

Fig. 3 Equivalent circuit of opening and closing coil loop

The theoretical waveform of the opening and closing coil current is shown in Fig. 4. The whole operation process of opening and closing coil can be divided into three stages: moving iron core start (0~t_0), moving iron core movement (t_0-t_1) and circuit breaker main actuator action (t_1-t_2).

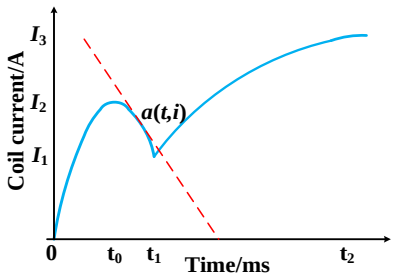

Fig. 4 Theoretical analysis waveform of coil current

III. COUPLING MULTIPHYSICS MODELING

The opening and closing coil system involves multiple physical quantities, which respectively describe the magnetic fields, circuit and dynamic characteristics of the system. The quantities are interrelated and affect each other.

Take any point A (t, i) in the t0-t2 phase of the current waveform in Fig. 4, and set the slope at A to k. The following equation can be obtained:

$$U = Ri + \frac{\mathrm{d}(Li)}{\mathrm{d}t} = Ri + L\frac{\mathrm{d}i}{\mathrm{d}t} + i\frac{\mathrm{d}L}{\mathrm{d}t} \quad (1)$$

$$= Ri + L\frac{\mathrm{d}i}{\mathrm{d}t} + i\frac{\mathrm{d}L}{\mathrm{d}x}\frac{\mathrm{d}x}{\mathrm{d}t} = Ri + Lk + i\frac{\mathrm{d}L}{\mathrm{d}x}\frac{\mathrm{d}F_x}{m}t$$

In equation (1), F_x is the external force exerted on the moving iron core, and m is the mass of the moving iron core.

The electromagnetic force, F_x, of the moving iron core can be calculated by the virtual displacement method. From the inductance formula, $L=N^2/R_m$, and the following equation can be obtained:

$$F_x = \frac{dW_m}{dx} = \frac{\phi^2}{2\mu_0 S_m} = \frac{(Ni)^2}{2\mu_0 S_m R_m^2} = \frac{(iL)^2}{2\mu_0 S_m N^2} \quad (2)$$

In equation (2), W_m is the magnetic field energy, Φ is the magnetic flux in the air domain within the coil, μ_0 is the permeability in a vacuum. S_m is the cross-sectional area of the air domain, and R_m is the total magnetic resistance of the equivalent magnetic circuit of the coil. N is the number of turns of the coil.

The magnetic field of the opening and closing coil can be divided into five areas as shown in Fig. 5, where area 1 is the magnetic field of the hollow core part of the coil, area 2 is the magnetic

International Journal of Advances in Engineering and Management (IJAEM)
Volume 4, Issue 2 Feb 2022, pp: 1279-1286 www.ijaem.net ISSN: 2395-5252

field of the moving iron core, and area 3-5 is the external magnetic field of the coil.

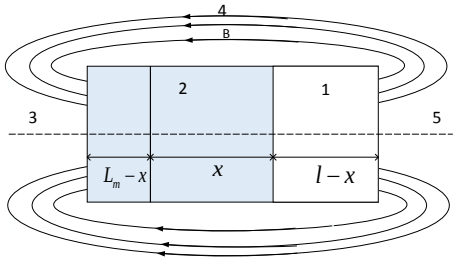

Fig. 5 Division of the magnetic field

In Fig. 5, L_m is the length of the moving iron core, and l is the length of coil. Aiming at area 1, the following can be obtained:

$$G=\frac{1}{R_m}=\frac{\boldsymbol{\Phi}}{F}=\frac{B_m S_m}{H_m L_m}=\mu\frac{S_m}{L_m} \quad (3)$$

In equation (3), G is magnetic conductance, F is the magnetic potential, and $F=Ni=\Phi R_m$. B_m is the magnetic density of region 1, and Hm is the magnetic field strength of region 1. μ is the magnetic permeability.

For area 2: Consider one end of the magnet as the "equivalent spherical pole" radiation [3], S and R are the cross-sectional area and radius of the moving iron core, respectively. The cylindrical permeance magnetized on the axis can be expressed as:

$$G=\mu_0\sqrt{\pi\cdot S}=\mu_0\sqrt{\pi\cdot\frac{1}{2}(2\pi R^2+2\pi RL_m)} \quad (4)$$

$$=\mu_0\pi\sqrt{R(R+L_m)}$$

For the calculation of the permeance outside the coil, the magnetic field outside the coil can be divided into countless permeance intervals. The permeance interval is separated by two planes with a certain angle, as shown in Fig. 6.

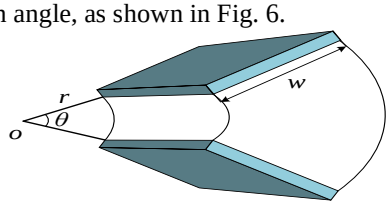

(a) when θ＜π

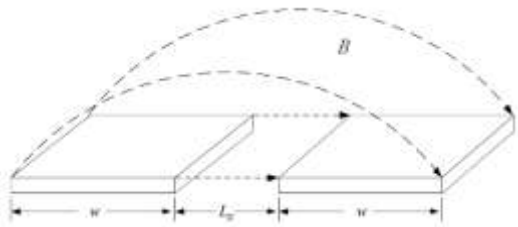

(b) when θ=π

Fig. 6 Permeability interval

The magnetic flux distribution in the area between the planes is not uniform. The area is divided into countless magnetic micro-elements with a cross-section of dS. The magnetic permeance of each micro-element is:

$$G=\mu_0\iiint_V\frac{dV}{L_p^2}=\mu_0\cdot\frac{w}{\theta}\ln(1+\frac{w}{r}) \quad (5)$$

L_p is the average length of magnetic micro-elements, and dV is the volume of each micro-element.

For area 3 and 5: Substitute w=100r=10D, θ=π/4, D is the coil diameter, into equation (5), then we can get:

$$G=\mu\cdot\frac{4w}{\pi}\ln(1+\frac{w}{r})=184.60\frac{\mu D}{\pi} \quad (6)$$

For area 4: Set θ=π and substitute $r=L_g/2$ into equation (5), L_g is the distance between the two planes when θ=π, then we can get:

$$G=\mu_0\cdot\frac{w}{\pi}\ln(1+\frac{2w}{L_g}) \quad (7)$$

The total magnetic resistance of the coil is:

$$R_m=\frac{1}{2}R_{m1}+R_{m2}$$

$$=(\frac{1}{\mu_{Fe}\pi(R(R+x)}+\frac{L_m-x}{\mu_0\pi\cdot R^2}) \quad (8)$$

$$+\frac{\pi}{2\mu_0}(5.47\times10^{-3}\cdot\frac{1}{D}+1.89\times10^{-3}\cdot\frac{1}{L_m})$$

In equation (8), R_{m1} and R_{m2} are magnetic resistance of region 1 and region 2, respectively. The following equations can be obtained:

$$\begin{cases} U_0=R_0 i+L\cdot k+i\cdot\dfrac{dL}{dx}\cdot\dfrac{F_x}{m}\cdot t \\ L=N^2\left[\begin{array}{l}(\dfrac{1}{\mu_{Fe}\pi\sqrt{R(R+x)}}+\dfrac{L_m-x}{\mu_0\pi\cdot R^2}) \\ +\dfrac{\pi}{2\mu_0}(5.47\times10^{-3}\dfrac{1}{D}+1.89\times10^{-3}\dfrac{1}{L_m})\end{array}\right]^{-1} \\ F_x=\dfrac{(iL)^2}{2\mu_0 S_m N^2} \end{cases} \quad (9)$$

In equation (9), L and F_x are respectively the inductance of the opening and closing coil and the electromagnetic force received by the moving iron core when the moving iron core displacement is x.

IV. SIMULATION

Establish a three-dimensional finite element model, which consists of a moving iron core, a connecting rod, a coil, a metal plate and a shell. Set the mesh division and region as shown in Fig. 7.

International Journal of Advances in Engineering and Management (IJAEM)
Volume 4, Issue 2 Feb 2022, pp: 1279-1286 www.ijaem.net ISSN: 2395-5252

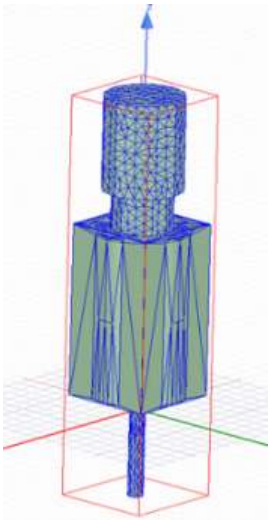

Fig. 7. Overall coil model and region settings

The model parameters are set as follows: the length of moving iron core is 60mm, the radius is 9mm, and the material is iron. The length of connecting rod is 40mm, the radius is 2mm, and the material is iron. Enameled wire is 56mm in length, 14.5mm in radius, the material is copper. The radius of wire section is 0.19mm, the number of coil turns is 147, and the resistance is 197.2Ω.

The function curve of coil current and time obtained by finite element simulation calculation is shown in Fig. 8. Take any 5 points on the AB section of the curve in Fig. 8 and record the abscissa and ordinate and slope of each point, which are described in Table 1.

Table 1 Data points of current-time curve

Mark point	X(ms)	Y(mA)	k(A/s)
P1	42.22	522.13	0
P2	44.95	493.52	35.24
P3	48.09	446.47	61.46
P4	50.24	390.96	75.71
P5	52.14	321.84	84.89

Substituting the data in Table 1 into equation (1), the displacement x, inductance L and electromagnetic attraction F_x at the five points A1~A5 are obtained through the three-dimensional transient multi-physics coupling system. The calculation results are shown in Table 2 below.

Table 2 Numerical analytical solutions of operating characteristics of the closing and opening coil

Mark point	L(mH)	x(mm)	F_x(N)
P1	9.56	0.12	0.05
P2	52.78	2.56	4.97
P3	238.1	8.97	13.49
P4	619.86	18.74	16.15
P5	3 113.21	34.88	50.31

V. OPTIMAL DESIGN

The optimal design of the opening and closing coil should be based on the premise that the impact trip device can be completed, and the goal is to appropriately increase the stroke force and reduce the opening and closing time. If the stroke force is too large, it will cause unnecessary energy waste and reduce the service life of the moving iron core and other opening and closing coil components; and if the opening and closing time is too short, it will generate a larger intercepting current, which will affect the safety and reliability of the power supply. It can be seen from formula (9) that, without changing the skeleton structure of the opening and closing coil, the opening and closing coil can be optimized for the number of turns N of the coil, the applied DC steady-state voltage U_0, and the magnetic material μ_{Fe}.

5.1 Number of turns of opening and closing coil

When the turns N of the opening and closing coil increases to K times, the dynamic inductance L will increase to K2 times the original value. According to the circuit analysis shown in Fig. 3, when the applied DC voltage U0 remains unchanged, the increase of the dynamic inductance L will cause the current i to decrease, and the finite element simulation software is used for analysis. Keep other parameters unchanged, and adjust the number of turns to 80%, 1.2 times, and 1.5 times of the original
parameters in turn, and the current waveform diagram is shown in Fig. 9.

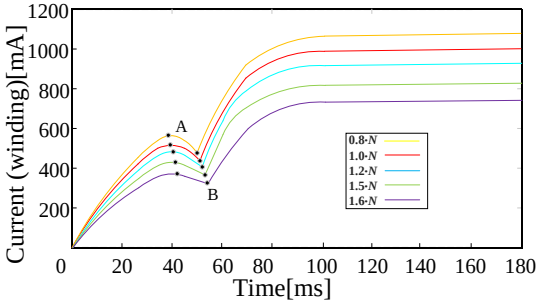

Fig. 9 Simulate current volatility under different turns

Substituting the current data under the conditions of the 5 types of turns in the Fig. 9 into equation (9), the characteristics of the opening and closing coils are shown in Table 3.

International Journal of Advances in Engineering and Management (IJAEM)
Volume 4, Issue 2 Feb 2022, pp: 1279-1286 www.ijaem.net ISSN: 2395-5252

Table 3 Operating characteristics of opening and closing coils under different turns

Turns N setting	Opening and closing time(ms)	Stroke force(N)
0.8· N	50.81	52.23
1.0· N	52.14	50.23
1.2· N	55.54	48.29
1.5· N	57.99	45.14
1.6· N	58.75	44.79

Therefore, within a certain range, the number of turns N of the opening and closing coils can be appropriately reduced, and the characteristics of the opening and closing coils can be optimized.

5.2 The magnetic material of the moving iron core

During the movement of the moving iron core, the choice of magnetic material will have a direct impact on the utilization of magnetic flux. The resistivity of the magnetic material will affect the magnitude of the induced eddy current in the iron core, and the magnetic permeability of the material will affect the magnitude of the magnetic field strength. Therefore, choosing low-conductivity and high-permeability materials can help increase the magnetic induction between the coil and the metal disk.

After comprehensively considering the electromagnetic properties of the material, the moving iron core materials are respectively selected cold-rolled silicon steel sheets and electrical pure iron[11] for simulation verification. Import the magnetic induction intensity, magnetic field intensity curve, multi-frequency iron loss curve, conductivity and other parameters of cold-rolled silicon steel sheet and electrical pure iron into the finite element simulation software to complete the properties of the magnetic materials. Some parameters of the magnetic material are shown in Table 4.

Table 4 some parameters of magnetic material

Material	Saturation magnetic induction B_s/T	Coercive force H_c/(A· m^{-1})	Conductivity σ/(S· m^{-1})	Maximum relative permeability μ
Electrician pure iron	2.14	32-96	10^7	4000-6000
Silicon steel sheet	2.00	12-31	2×10^6	7000-15000

Keep other parameters unchanged, and adjust the moving iron core material to electrical pure iron and silicon steel sheet in order to obtain the current waveform as shown in Fig. 10.

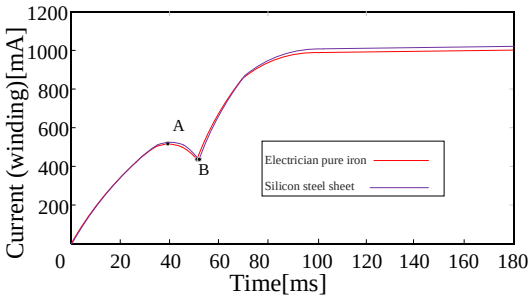

Fig. 10 Simulate current volatility under different magnetic materials

Substituting the current data under the conditions of the two moving iron core materials in Fig. 10 into equation (9), the characteristics of the opening and closing coils are shown in Table 5.

International Journal of Advances in Engineering and Management (IJAEM)
Volume 4, Issue 2 Feb 2022, pp: 1279-1286 www.ijaem.net ISSN: 2395-5252

Table 5 Operating characteristics of opening and closing coils under different magnetic materials

Material	Opening and closing time(ms)	Stroke force(F)
Electrician pure iron	52.14	50.23
Silicon steel sheet	51.55	52.94

From the above analysis, it can be known that low-conductivity and high-permeability materials can be selected to optimize the characteristics of the opening and closing coils.

5.3 Applied DC steady-state voltage U_0

Keep other parameters unchanged, and adjust the applied DC steady-state voltage U_0 to 50%, 80%, and 1.2 times of the original parameters, respectively, and the current waveform diagram is shown in Fig 11.

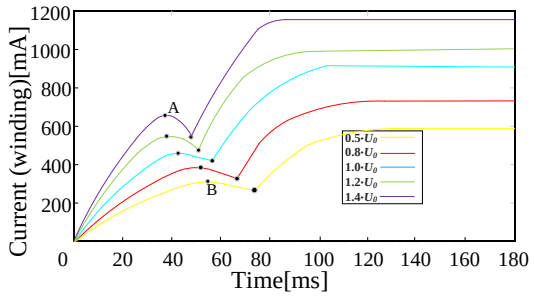

Fig. 11 Simulate current volatility under different applied DC steady-state voltage U_0

Substituting the current data under the conditions of the 5 types of external DC steady-state voltages U0 in the Fig 11 into equation (9), the characteristics of the opening and closing coils are shown in Table 6.

Therefore, within a certain range, the external DC steady-state voltage U0 can be appropriately increased to achieve the optimization of the opening and closing coil characteristics.

TABLE 6 Operating characteristics of opening and closing coils under different external DC steady-state voltages U_0

Voltage U_0 setting	Opening and closing time(ms)	Stroke force(F)
0.5· U_0	77.32	38.69
0.8· U_0	62.13	48.34
1.0· U_0	55.14	50.23
1.2· U_0	53.30	54.64
1.4· U_0	47.90	65.35

VI. VERIFICATION

Set up the experimental platform as shown in Fig. 12, which is used to measure the current waveform. The platform is divided into 3 parts, namely the motion part, the circuit part and the monitoring part. The motion part is the analog device for the opening and closing mechanism of the high-voltage circuit breaker. The circuit part adopts IT6514D DC stabilized power supply to provide DC voltage for the opening and closing coil loop. The monitoring part includes the current sensor, data acquisition device and the upper computer, which sends the opening or closing operation instructions to the operating device and collects the current of the opening and closing coils.

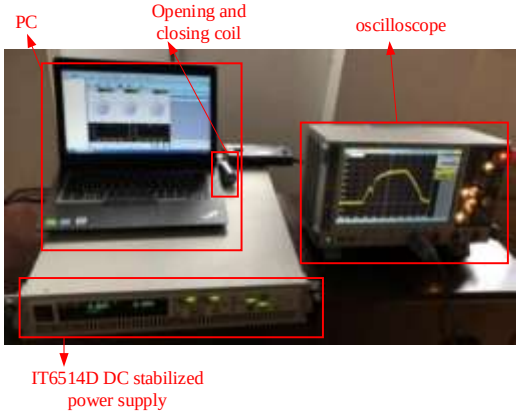

Fig.12 Opening and closing time detection

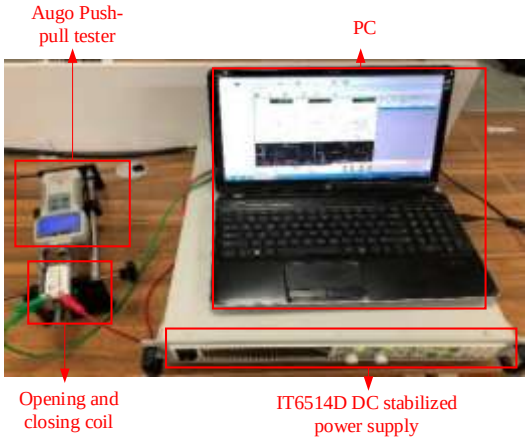

Fig. 13 Stroke-force detection

International Journal of Advances in Engineering and Management (IJAEM)
Volume 4, Issue 2 Feb 2022, pp: 1279-1286 www.ijaem.net ISSN: 2395-5252

The experimental platform shown in Fig. 13 is used for stroke-force test of moving iron core, and the Augo push-pull tester is on the left side of the platform.

The current waveform captured by the sensor is imported into the PC through the PicoScope data acquisition system for filtering processing, as shown in Fig. 14. The theoretical points and simulation curves are also plotted in Fig. 14.

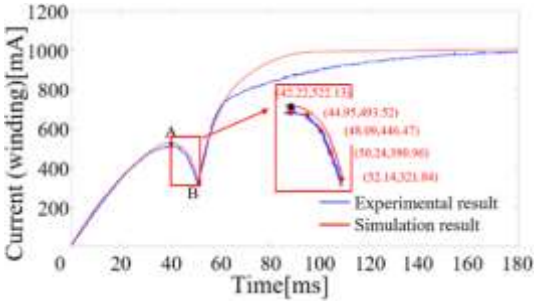

Fig. 14 Experimental current sampling waveform

We can see that in Fig.14, the difference between experiment and simulation mainly exists for a period of time after point B. In the ideal environment of simulation, after the iron core hits the metal plate, the magnetic circuit composed of the iron core, metal plate and shell is short-circuited, the iron core is easily saturated, and the inductance of the coil is reduced accordingly. Thus, the current in the coil increases rapidly and soon reaches a stable state. On the other hand, in the experiment, the iron core will not be saturated, so the measured current waveform rises slowly compared with the simulation current waveform. However, this part of the current waveform does not affect the analysis of the operating characteristics of the opening and closing coils, which can be ignored in this research.

The simulation and experimental results of stroke force at the end of stroke and opening and closing time are shown in Table 7 and Table 8 respectively.

TABLE 7 Comparation results of stroke force at the end of stroke

Experiment force(N)	**Simulation force(N)**	**Relative error (%)**
	53.88	3.45
55.86	**Calculated force(N)**	**Relative error (%)**
	52.31	6.36

TABLE 8 Comparation results of opening and closing time

Experiment time(ms)	**Simulation time(ms)**	**Relative error (%)**
	52.14	5.57
49.39	**Calculated time(ms)**	**Relative error (%)**
	52.19	5.67

VII. CONCLUSIONS

In this paper, a three-dimensional finite element simulation model is established of the circuit breaker opening and closing coil. Compared with the experimental results, the relative error between the simulation and experimental results of the force at the end of the stroke is 3.54%, and the opening and closing time is 5.57%, which proves the feasibility and effectiveness of the finite element simulation modeling method presented in this paper.

In addition, based on theory and simulation, this article puts forward some optimization suggestions of the opening and closing coils. Under the condition that other structural parameters remain unchanged, appropriately reducing the number of opening and closing coil turns N and increasing the applied DC steady-state voltage U_0 can improve the operating characteristics of the opening and closing coils. The moving iron core selection of low conductivity and high permeability materials will help reduce the eddy current loss of the opening and closing coils, and improve magnetic flux utilization.

REFERENCES

[1]. Wang Jianhua, et al. The latest technology research and application development prospects of smart appliances [J]. Transactions of the China Electro technical Society, 2015, 30(09):1-11.

[2]. Kotra S, MISHRA M K. Design and Stability Analysis of DC Microgrid with Hybrid Energy Storage System [J]. IEEE Transactions on Sustainable Energy, 2019(99): 1-1.

[3]. Peng C, Husain I. Evaluation of design variables in Thompson coil based operating mechanisms for ultra-fast opening in hybrid AC and DC circuit breakers[C]. Applied Power Electronics Conference & Exposition. IEEE, 2015.

[4]. Chu Feihang, et al. Research on the degradation law of 252 kV circuit breaker opening and closing coils under environmental factors [J]. Electric Power

Automation Equipment, 2021, 41(02): 218-224.

[5]. Li Fuxing, et al. High-voltage circuit breaker mechanical state detection based on optimized VMD [J]. Electric Power Automation Equipment, 2018, 38(11): 148-154.

[6]. Geng Yaming. Research on live detection and fault diagnosis of operating characteristics of circuit breaker spring operating mechanism [D]. North China Electric Power University (Beijing), 2017.

[7]. Huang Xinbo, Hu Xiaowen, Zhu Yongcan, Wei Xueqian, Zhou Yan, Gao Hua. High-voltage circuit breaker fault diagnosis based on convolutional neural network algorithm [J]. Electric Power Automation Equipment, 2018, 38(05): 136-140+147.

[8]. Sun Shuguang, et al. Diagnosis on the Switching Fault of Conventional Circuit Breaker Based on Vibration Signal Sample Entropy and RVM [J]. Transactions of China Electro technical Society, 2017, 32(7): 20-30.

[9]. Ruan Jiangjun, Yang Qiuyu, et al. Morphological characteristics of chaotic attractors for mechanical vibration signals of high-voltage circuit breakers [J]. Electric Power Automation Equipment, 2020, 40(03): 187-193.

[10]. Li Pengfei, et al. The Dynamic Characteristics and Energy Storage State Detection Method of High-voltage Circuit Breaker Closing Spring [J]. Transactions of China Electro technical Society, 2016, 31(3): 104-111.

[11]. Li Xiaolin, et al. The influence of magnetic materials on the output efficiency of electromagnetic repulsion mechanism[J]. High Voltage Technology, 2020, 46(02): 586-593.